Enabling the use of unstructured meshes for the Large Eddy Simulation of stable atmospheric boundary layers

Ulysse Vigny[a,b], Léa Voivenel[c], Mostafa Safdari Shadloo[b,d], Pierre Bénard[b], Stéphanie Zeoli[a]

[a]*Fluid Machine Unit, University of Mons (UMONS), Mons, 7000, Belgium,*
[b]*INSA Rouen Normandie, Univ Rouen Normandie, CNRS, Normandie Univ, CORIA UMR 6614, F-76000 Rouen, France,*
[c]*CNRS, INSA Rouen Normandie, Univ Rouen Normandie, Normandie Univ, CORIA UMR 6614, F-76000 Rouen, France,*
[d]*Institut Universitaire de France, Rue Descartes, F-75231 Paris, France,*

Abstract

Modeling wind flows in complex terrain under varying atmospheric stability conditions is valuable to better understand its physics and impacts on wind turbines. Yet their numerical simulations are still challenging. Stable boundary layer (SBL) are difficult to model, mostly due to the small size of the characteristic eddies. Complex terrain are hard to match with structured grids. Such constrains require both high fidelity simulations at high resolution and unstructured meshes. This work presents an original numerical framework answering these requirements. It is then validated against the GABLS1 benchmark, a $400 \times 400 \times 400\,\mathrm{m}^3$ box with periodic walls, cooled by the bottom where surface temperature decrease over time. Induced wall heat flux generates thermal stratification and thus a stable boundary layer. Results with structured and unstructured grids are satisfactory, with both simulations being within the dispersion of previous studies. Minor differences are highlighted. Due to the grid quality, the order of the numerical schemes and the accuracy of the flux estimation, unstructured grids simulations have higher wall heat fluxes than structured grids ones. This gap widens over time, reaching 14%, impacting velocity, temperature, variances and fluxes. Stable boundary layer is found to be around 10% higher. The grid resolution employed highly impacts the accuracy of the SBL modeling. A mesh refine-

Email address: `ulysse.vigny@umons.ac.be` (Ulysse Vigny)

Preprint not peer reviewed

This preprint research paper has not been peer reviewed. Electronic copy available at: https://ssrn.com/abstract=4995353

ment study has been carried out with both structured and unstructured grids showing that a $\Delta x = 6.25\,\mathrm{m}$ grid size is sufficient to correctly reproduce the stable boundary layer.

Keywords: GABLS1, Large-eddy simulations, Stable boundary layer, Unstructured grids

1. Introduction

Given today's energy and environmental challenges, increasing the electrical power generated by wind farms is of paramount importance [1]. To this end, the size of wind turbines has significantly increased over the years, with rotors reaching hundreds of meters in diameter. The aforementioned wind turbines are no longer affected solely by micro-scale wind flows that extend well below 1 km. They are also affected by meso-scale processes, ranging from 5 to hundreds of kilometres in size, which influence local weather. They are at the interface between the micro- and meso-scale [2].

The expansion of the scale introduces novel phenomena that modify the overall flow physics. At altitude, we find the geostrophic wind as a result of the balance between the pressure gradient force and the Coriolis force. While pressure gradient is induced by weather systems such as low- or high-pressure areas, Coriolis force is a consequence of the Earth angular momentum conservation. At intermediate heights, we find phenomena that induce a change in the atmospheric boundary layer (ABL) structure. The best known is the thermal stratification. Due to sun's heat, air density varies alternating buoyancy forces. This phenomenon can be either stable or unstable, depending on the direction of the vertical thermal gradient [3].

Finally on the ground, we find terrain effect, which influences horizontal and vertical velocity gradients. Complex terrain can also induce flow separation, re-circulation and roughness change. A finer comprehension of the physics underlying the previously described phenomena is required to better predict the behaviour of wind turbines in complex environments. However, the knowledge of wind flows in such complex environments remains incomplete [2].

This study aims to address this challenge by focusing on one specific aspect: thermal stratification. It is well established that wind turbines performances are significantly influenced by wind shear, with implications on wake recovery, speed deficit, induced turbulence, energy production, loads

Preprint not peer reviewed

This preprint research paper has not been peer reviewed. Electronic copy available at: https://ssrn.com/abstract=4995353

and fatigue [4]. To gain insight into these phenomena, field measurement campaigns and wind tunnel experiments can be conducted [5, 6]. Their use remains constrained by their inherent complexity as well as by the costs associated to their implementation. In this context, there has been a growing tendency to rely on numerical simulations as a means of investigation [7]. Nevertheless, while simulations of the convective boundary layer (CBL) has been wildly performed [7], accurate simulation of the stable boundary layer (SBL) remains a challenging task [7]. The main difficulty lies in the capture of characteristic vortices, which can be particularly small. Indeed, the height of the atmospheric boundary layer varies considerably depending on the thermal stratification [8]. While a CBL can reach altitudes of approximately 1 km, an SBL is approximately 200 m high. Additionally, CBLs are driven by large convection vorticies, which generate further turbulence. In contrast, SBLs are driven by wind shear and exhibit lower levels of turbulent kinetic energy. As a result of their reduced height and turbulence, their vorticies characteristic size are also smaller. To accurately capture these features, high spacial resolution is needed, leading in large computational resources requirements. The state-of-the-art tool to enable precise numerical prediction of stable boundary layer flows is the Large Eddy Simulation (LES) technique [7].

To enhance comprehension of stable boundary layers by Large Eddy Simulation (LES), the Global Energy and Water Cycle Experiment (GEWEX) initiated the GEWEX Atmospheric Boundary Layer Study (GABLS). The objective was to enhance comprehension of stable boundary layer and improve its representation by LES models [9]. The focus of GABLS has been on SBLs over land and the representation of diurnal cycle. Three different GABLS intercomparisons have already been carried out, focusing on progressively more realistic cases. These benchmarks are considered important for improving the modeling of stable atmospheric layers [10]. In this work, we consider the GABLS1 benchmark targeting an idealized Arctic stable boundary layer case [11].

Initially, a comparison of 11 LES codes was carried out [12]. The GABLS1 setup consists of a periodic box with an uniform initial velocity profile, cooled by the bottom wall, where the surface temperature decreases over time. The study has shown that the grid resolution employed highly impacts the accuracy of the SBL modeling. A range of mesh resolution has been given in order to correctly capture the flow physics behaviour. Subsequent to the initial study, several LES have been conducted employing the GABLS1 con-

Preprint not peer reviewed

This preprint research paper has not been peer reviewed. Electronic copy available at: https://ssrn.com/abstract=4995353

figuration with the objective of replicating an SBL scenario. The benchmark results are used to validate the underlying framework, as well as to investigate the influence of finer grid [13, 14], surface cooling rate [13, 15, 16] or subgrid-scale (SGS) [17, 18, 19] impact. Other studies have used the GABLS1 configuration to validate their Reynolds Averaged Navier-Stokes equations (RANS) or pseudo-spectral methods [10, 20]. Regardless of the approach employed, all of these studies accurately reproduce the physical behaviour of the stable boundary layer, but the use of finer grids does not prejudge the quality of the results. It is worth mentioning that all the aforementioned studies were conducted on structured grids. None have used unstructured grids since the domain was not requesting.

The simulation of wind flows in complex terrain is also a challenging topic due to the difficulty of creating a mesh that accurately reflects the topography [2]. Structured meshes, which are commonly used in atmospheric flow simulations, tend to encounter difficulties when attempting to follow complex geometries. For this reason, the use of unstructured grid is mandatory. However, the complexity of developing high-order flow solvers for unstructured meshes has limited their use in real atmospheric studies. To address the reluctance of the research community to employ such meshes, it is essential to validate their use in simple scenarios before progressing to more complex studies. Therefore, the aim of this study is to draw analogous conclusions for simulations using unstructured grids. To the author's knowledge, a Large Eddy Simulation of a stable boundary layer has never been performed on an unstructured grid, and this work aims to address this gap in the literature. Conclusions on the minimum and optimum mesh size [12] for robust LES are drawn using only a structured grid.

The manuscript is structured as follows: the methodology is described in Section 2. Section 3 first presents the GABLS1 stable boundary layer results obtained with both structured and unstructured grid having an identical grid length. Then a sensitivity to resolution study is carried out in the same section. Finally, conclusions are drawn in Section 4.

2. Methodology

2.1. GABLS1 configuration

The GABLS1 intercomparison is based on an idealized Arctic stable boundary layer case [11]. A domain of $400 \times 400 \times 400\,\mathrm{m}^3$ with periodic walls on both streamwise, X, and tengential, Y, direction is employed. The

Preprint not peer reviewed
This preprint research paper has not been peer reviewed. Electronic copy available at: https://ssrn.com/abstract=4995353

bottom boundary condition is a rough wall with a $z_0 = 0.1\,\mathrm{m}$ roughness. The surface temperature is $T_w = 265\,\mathrm{K}$ with a cooling rate of $0.25\,\mathrm{K.h^{-1}}$. The top boundary condition is a sleep wall. An imposed uniform geostrophic wind of $G_x = 8\,\mathrm{m.s^{-1}}$ in the east-west direction at latitude 73° north drives the stable boundary layer, corresponding to a Coriolis parameter of $f = 1.39 \times 10^{-4}\,\mathrm{s^{-1}}$. Gravity, reference potential temperature and density as well as the Von Karman constant are set to $g = 9.81\,\mathrm{m.s^{-2}}$, $\theta_0 = 263.5\,\mathrm{K}$, $\rho_0 = 1.3223\,\mathrm{kg.m^{-3}}$ and $\kappa = 0.4$, respectively. Figure 1 illustrates the configuration of the GABLS1 setup.

Initial velocity profile is set to geostrophic wind, i.e. a uniform $u_x = 8\,\mathrm{m.s^{-1}}$ velocity profile. Initial vertical temperature profile is set uniform to $265\,\mathrm{K}$ in the first hundred meters and then increases by $0.01\,\mathrm{K.m^{-1}}$ up to the top of the domain, reaching $268\,\mathrm{K}$ at the top. Random perturbations are introduced in the first fifty meters with a $0.1\,\mathrm{K}$ amplitude as specified in [12].

To mitigate gravity-wave reflexion, a sponge layer (SL) is applied above three hundred meters. In order to smoothly relax the velocity and the temperature and thus avoid numerical errors, the sponge layer follows:

$$SL_\phi = \gamma \times \sin^2\left(\frac{z - Z_{SL}}{L_z - Z_{SL}} \times \frac{\pi}{2}\right) \times (\phi_{target} - \phi)\,, \tag{1}$$

where ϕ is the actual velocity or temperature. Here, ϕ_{target} is the target velocity or temperature, set to geostrophic wind or linear increasing temperature respectively. $\gamma = \frac{1}{5}$ is a time relaxation parameter and z is the height varying between the SL bottom height $z_{SL} = 300\,\mathrm{m}$ and the domain top height $z_{top} = 400\,\mathrm{m}$. The sponge layer is then smoothed over time and over space.

2.2. Flow solver

LES are performed with the incompressible flow at constant density solver from the YALES2 platform [21]. YALES2 is a massively parallel finite volume flow library able to process structured and unstructured meshes. Spatial fourth-order central scheme and time fourth order Runge-Kutta-like integration method are used [22]. In this work we solve the filtered Navier Stokes equations, expressed using Einstein's notation where $\tilde{\bullet}$ is the low-pass spatial filtering operator, as:

Continuity equation

$$\frac{\partial \tilde{u}_i}{\partial x_i} = 0\,, \tag{2}$$

Preprint not peer reviewed
This preprint research paper has not been peer reviewed. Electronic copy available at: https://ssrn.com/abstract=4995353

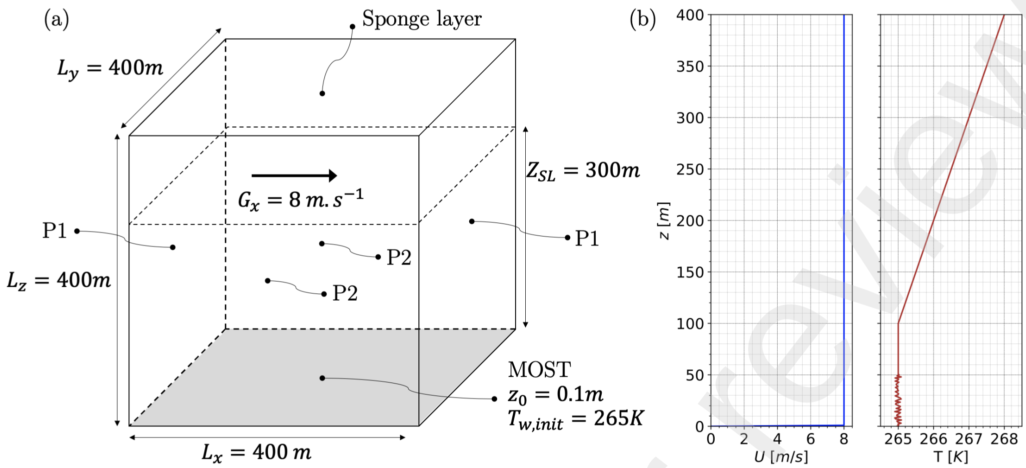

Figure 1: (a): GABLS1 setup configuration scheme. $P1$ and $P2$ for periodic walls in pairs. (b): intial velocity and temperature vertical profiles.

Momentum-conservation equation

$$\frac{\partial \tilde{u}_j}{\partial t} + \frac{\partial \tilde{u}_i \tilde{u}_j}{\partial x_i} = \nu \frac{\partial^2 \tilde{u}_j}{\partial x_i \partial x_i} + \frac{1}{\rho_0}\frac{\partial}{\partial x_i}\tau_{ij}^R - \frac{1}{\rho_0}\frac{\partial \tilde{P}}{\partial x_j} + \frac{\tilde{\rho} g}{\rho_0} - 2\Omega(G_i - \tilde{u}_i)\,, \quad (3)$$

where u is the fluid velocity, ν the kinematic viscosity, ρ_0 the reference air density, τ_{ij}^R the residual stress tensor and P the pressure. The last two terms are the Boussinesq approximation [23] to account for the gravitational effect induced by thermal stratification and the Coriolis effect, respectively. In these terms, ρ is the local density, g the Earth gravitational constant, Ω the Earth angular velocity and G is the geostrophic wind.

2.3. Wall model

As the mesh resolution is not enough to capture the boundary layer, one must employ a wall model in order to predict momentum and heat flux at the wall. The most common atmospheric flow wall model is based on the Monin-Obukhov Similarity Theory [24, 25] and assumes classical logarithmic profiles for both temperature and velocity. It is capable of accommodating all three atmospheric thermal configurations: neutral, stable, and unstable. This is made possible by the presence of correction terms whose intensity and shape vary depending on the thermal state [3].

Preprint not peer reviewed
This preprint research paper has not been peer reviewed. Electronic copy available at: https://ssrn.com/abstract=4995353

The velocity and temperature profiles can be expressed as follows:

$$\frac{\bar{u}(z)}{u_*} = \frac{1}{k}\left[\ln\left(\frac{z}{z_0}\right) - \psi_m\left(\frac{z-z_0}{L}\right)\right], \tag{4}$$

$$\frac{\theta(z)-\theta_w}{\theta_*} = \frac{1}{\kappa}\left[\ln\left(\frac{z}{z_0}\right) - \psi_h\left(\frac{z-z_0}{L}\right)\right], \tag{5}$$

where $u_* = \sqrt{\tau_w/\rho}$ is the friction velocity with τ_w the local shear stress at the wall. $\theta_* = -q_w/u_*$ is the friction temperature where q_w is the kinematic surface heat flux and θ_w is the wall temperature. κ is the Von Karman constant and z_0 the roughness length. L the Obukhov length which represents the height above the surface from where buoyancy first dominates shear computed as $L = -\frac{u_*^3\theta_0}{\kappa g q_w}$. $\theta_0 = 263.5\,\mathrm{K}$ is the reference potential temperature.

The correction functions ψ_m and ψ_h are set to zero for neutral cases, leading to a classical logarithmic velocity profile. For non-neutral configurations, they can be expressed as:

$$\psi_{m/h}(\xi) = \int_{z_0/L}^{\xi} \frac{1-\phi_{m/h}(\xi)}{\xi}\,\mathrm{d}z\,, \tag{6}$$

where $\xi = z/L$. Furthermore, ϕ_m and ϕ_h are referred to as the stability functions. They are empirically determined and can be expressed depending on the stability condition as:

Unstable cases

$$\begin{aligned}\phi_m &= (1-\gamma_m\xi)^{-1/4}\,,\\ \phi_h &= (1-\gamma_h\xi)^{-1/2}\,,\end{aligned} \tag{7}$$

Stable cases

$$\begin{aligned}\phi_m &= 1+\beta_m\xi\,,\\ \phi_h &= 1+\beta_h\xi\,,\end{aligned} \tag{8}$$

Various parameterizations were introduced over the years [26, 27]. In this work, we use the one prescribed in the GABLS1 setup: $\beta_m = 4.8$ and $\beta_h = 7.8$.

As mention in [28], surface temperature is prescribed as boundary condition instead of surface sensible heat flux. Thus we have a two-unknown

Preprint not peer reviewed

This preprint research paper has not been peer reviewed. Electronic copy available at: https://ssrn.com/abstract=4995353

Mesh name	S1	U1	S2	U2	S3	U3	S4	U4
Δx [m]	12.5		6.25		3.125		2.0	
N_{elem} [$\times 10^3$]	32.8	148.2	262.1	1186	2097.2	9487.9	8000.0	35972.8
N_{node} [$\times 10^3$]	45.4	41.8	366.3	337.8	2919.7	2659.1	11255.5	10042.7
Δt [s]	0.2		0.1		0.05		0.032	

Table 1: Case set-up with Δx the mesh cell size, N_{elem} the number of mesh elements and Δt the time step.

problem, u_* and q_w. We therefore use a double Newton-Raphson convergence method [29] for its quadratic convergence speed.

As wall models are derived from averaged Navier-Stokes equations, quantities such as velocity and temperature must be spatially filtered [30]. For structured grids, averaging the quantities on the horizontal plane passing through the $1st$ node is straightforward. For unstructured grids, the $1st$ node plane does not exist. To overcome this problem a filtering operator is applied to the latter as well as to the first node velocity and temperature used to build the momentum and heat flux at the wall.

2.4. Numerical set-up

Structured (S) and unstructured (U) meshes with 4 different resolutions are used in this study. Tab. 1 gathers the mesh characteristics for these cases. The number of elements varies significantly between the structured and unstructured meshes of the same resolution but the number of nodes is similar. Since the control volumes are defined at the nodes into YALES2, the number of degrees of freedom remains approximately the same and so the mesh type comparison is fair.

Subgrid scale modelling is performed using the dynamic Smagorinsky model [31, 32]. Even though different models are sometimes used to better model anisotropic flows [19], Smagorinsky models are still the most commonly used in the literature and has been proven to perform reasonably well [33]. In addition, dynamic Smagorinsky model has shown to be more effective at sustaining deeper SBLs relative to the Smagorinsky model [12].

Simulations are ran out for a total of 8 hours of physical time, representing a diurnal cycle. Statistics are collected on the last hour i.e. between the $7th$ and the $8th$ hour. Our results are compared with the eleven LES codes from

Preprint not peer reviewed
This preprint research paper has not been peer reviewed. Electronic copy available at: https://ssrn.com/abstract=4995353

the first GABLS1 intercomparison [12] but also with various studies who compared themselves to the first study [15, 16, 17, 13, 34, 18, 19, 35].

2.5. Time discretization

Flow solver time step is here imposed to respect the Courant-Fredrichs-Lewy $CFL = U\Delta t/\Delta x$ condition. Due to the explicit integration of the Coriolis force, the time step is chosen following [36] such that $\Delta t = \frac{CFL \times \Delta x}{\|U\| + \sqrt{gH}}$ with H the vertical depth of the fluid, i.e. the stable boundary layer height. The imposed time step is evaluated to ensure $CFL < 0.9$ with a convective velocity $\|U\| = 9\,\mathrm{m.s}^{-1}$ and a boundary layer height $H = 200\,\mathrm{m}$. All time steps used in this study are summarized in Table 1.

3. Results

3.1. Unstructured and Structured grid comparison

To validate the use of unstructured meshes for the simulation of atmospheric flows, the first step is to assess the mesh type impact by comparing results from both unstructured and structured grids. The mesh resolution is chosen as advised by [12] to be optimal for robust LES, i.e. $\Delta x = 3.125\,\mathrm{m}$ for an isotropic grid. Grids are referred as $S3$ and $U3$ for structured and unstructured grids, respectively, according to Tab. 1.

Time series of frictional velocity, wall heat flux and Monin-Obukhov length are shown in Fig. 2. All of these variables fall within the dispersion envelope of the original GABLS1 study results [12]. As far as the frictional velocity is concerned, the results are quite similar for both kind of grids even if the $S3$ grid results are slightly lower. Particularly interesting, the $U3$ results fit its counterpart obtained with the state-of-the-art and commonly used tool PALM [35].

The same observation can be made for the Monin-Obukhov length, which is similar for both grids. After a strong decrease during the first hour, it quickly converges to $O(100)\,\mathrm{m}$. Wall heat fluxes for the $S3$ and $U3$ cases exhibit similar physical behaviour and decrease with time due to the cooling rate. However, a gap starts developing after 1 h, reaching a maximum between the $7th$ and $8th$ hour where a 14% average wall heat flux difference is measured. This gap could be explained by a numerical effect of the mesh type. Some time after the initialisation where the flow is laminar, a flow destabilization process occurs leading to the development of the stable turbulent boundary layer. This development is directly impacted by the initial

Preprint not peer reviewed

This preprint research paper has not been peer reviewed. Electronic copy available at: https://ssrn.com/abstract=4995353

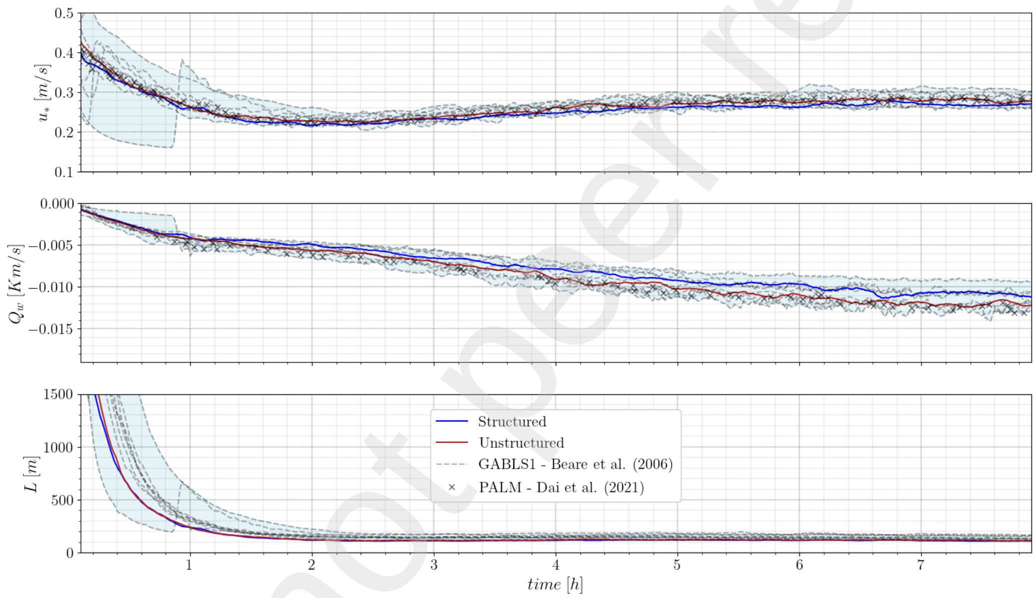

Figure 2: Frictional velocity, wall heat flux and Monin-Obukhov length with $S3$ and $U3$ grids, compared to original GABLS1 results dispersion [12] and PALM results [35].

Preprint not peer reviewed

This preprint research paper has not been peer reviewed. Electronic copy available at: https://ssrn.com/abstract=4995353

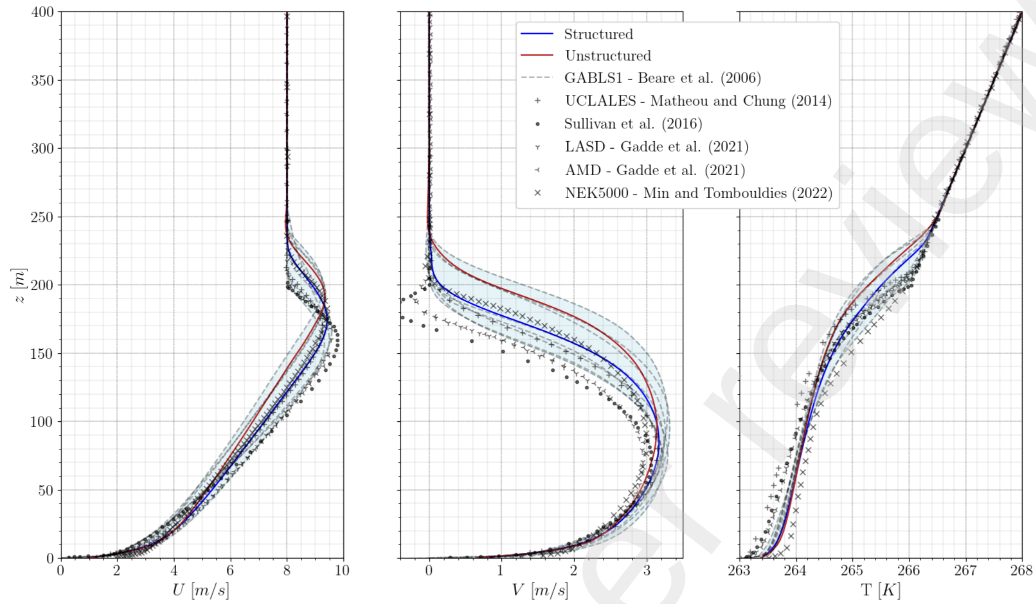

Figure 3: Streamwise and tangential velocities and temperature profile for meshes $S3$ and $U3$ with cell size $\Delta x = 3.125\,\mathrm{m}$. Blue shaded area stands for the original GABLS1 study results dispersion [12] and symbols for more recent studies [17, 13, 19, 14].

temperature field which contains random values, and so is different from one simulation to another. More information on these sources of errors are given into Appendix 4. This destabilisation process could also explain the strong jump in some GABLS1 original results of Fig. 2. Consequently, mesh type and resolution will have an impact on the flow development which cannot converge to the same results since the boundary conditions are unsteady.

Following the GABLS1 recommended post-processing procedure, the profiles are spatially averaged over horizontal planes and temporally averaged between the $7th$ and $8th$ hour. The streamwise velocity U, tangential velocity V and temperature T profiles are plotted in Fig. 3 and compared to the original GABLS1 results [12] as well as more recent studies [17, 13, 35, 19, 14]. The streamwise velocity is zero at the bottom of the domain and is set to the geostrophic wind at the top. The stable boundary layer is developed with a velocity peak between 160 and 200 m. The tangential velocity, being zero in the geostrophic wind, starts to grow by descending into the domain due to the Coriolis effect. In the vicinity of the wall, where the friction effect is

Preprint not peer reviewed

This preprint research paper has not been peer reviewed. Electronic copy available at: https://ssrn.com/abstract=4995353

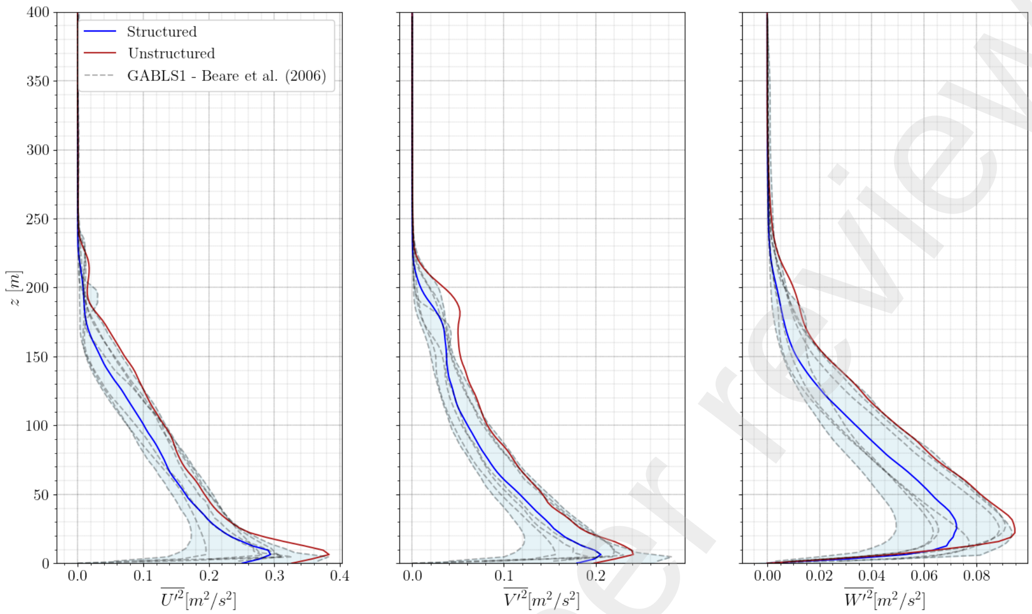

Figure 4: Streamwize, tangential and vertical velocity variances with $S3$ and $U3$ of cell size $\Delta x = 3.125$ m. Blue shading stands for the original GABLS1 study results dispersion [12].

dominant, the tangential velocity is reduced to zero. The temperature profile shows a behaviour correlated with both velocity profile with an increase with height and a bend between 150 and 200 m. All three profiles show differences between $S3$ and $U3$ simulations but remain within the dispersion of the GABLS1 results. The $U3$ simulation has a streamwise velocity peak offset of 20 m compared to $S3$, also visible on the tangential velocity profile and on the temperature inflection point. More recent studies are also compared, most of which show a similar behaviour but also expand the original results dispersion. For example, Sullivan [13] exhibits an unexplained negative tangential velocity near the top of the boundary layer. This results spreading enlargement show the difficulty in having reference data but assure some confidence in our results with both meshes.

Variance of streamwize $\overline{U'^2}$, tangential $\overline{V'^2}$ and vertical $\overline{W'^2}$ velocities are plotted in Fig. 4. All three velocity variances are zero in the geostrophic region due to the imposition of the sponge layer and increase by decreasing the height. In the vicinity of the wall the variances dampen through the wall model impact. For all three components, the $U3$ configuration always shows

Preprint not peer reviewed
This preprint research paper has not been peer reviewed. Electronic copy available at: https://ssrn.com/abstract=4995353

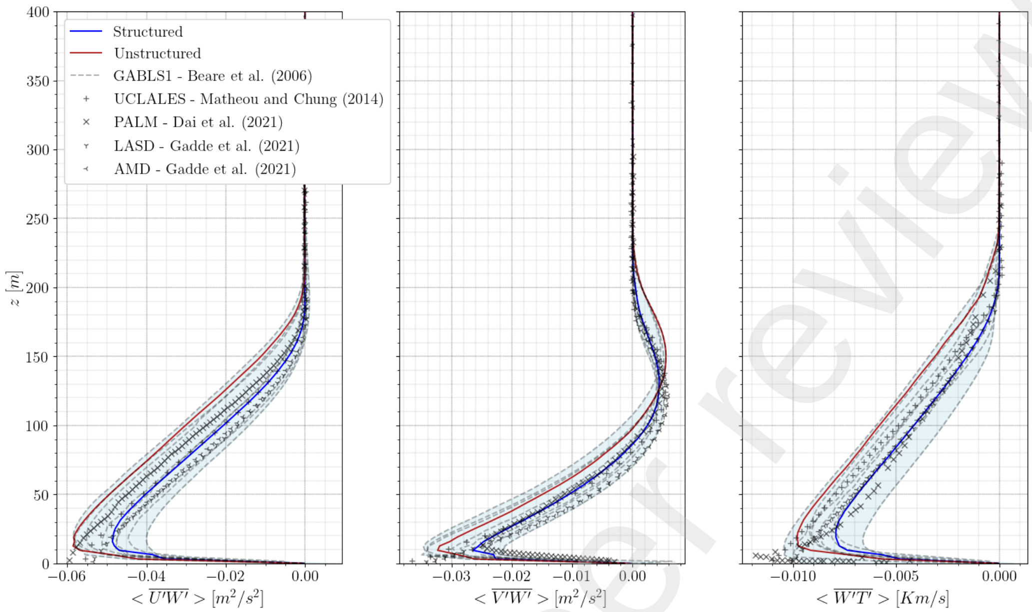

Figure 5: Momentum and heat fluxes for meshes $S3$ and $U3$ with cell size $\Delta x = 3.125\,\mathrm{m}$. Blue shading stands for the original GABLS1 study results dispersion [12] and symbols for more recent studies [17, 35, 19].

higher values than $S3$, regardless of the ground distance, showing a higher fluctuation level with the unstructured mesh.

The momentum fluxes $\langle\overline{U'W'}\rangle$, $\langle\overline{V'W'}\rangle$ and the heat flux $\langle\overline{W'T'}\rangle$ are plotted in Fig. 5. Similar global behaviour is observed for all fluxes. Nevertheless, a similar vertical offset for the $U3$ mesh compared to $S3$ is observed, here due to the higher level of fluctuations. These results are again well within the GABLS1 scatter and similar to recent studies.

To summarize, both $S3$ and $U3$ simulations bring similar results as other studies, even though differences are noticeable among them. Firstly, the temperature profile presents a lower temperature inflection. This gap is the source of the difference in the averaged velocity profile. Secondly, a lower wall heat flux, but higher in norm, generates more turbulent kinetic energy and thus more velocity variances.

The gap on heat flux profile might be the cause of the total wall heat flux time deviation. Indeed, a different momentum flux at the wall implies a different scalar flux, thus a different wall heat flux. Three causes have been identified for this phenomenon: the grid quality, the order of the numerical

Preprint not peer reviewed

This preprint research paper has not been peer reviewed. Electronic copy available at: https://ssrn.com/abstract=4995353

schemes and the accuracy of the flux estimations. For the grid quality, both grids have the same characteristic cell size but not the same quality. As the $S3$ mesh is structured and possesses uniform hexahedron, its quality is good and homogeneous. On the contrary, the $U3$ grid is unstructured and so each tetrahedron constituting the mesh can vary locally.

Grid quality can be evaluated via the skewness parameter, which measures the deviation between the existing cell and an optimal cell. Figure 6 shows the $U3$ grid skewness distribution. The $U3$ skewness is mainly arround 0.3, but reaches locally values of 0.96 with 0.5% of elements with a skewness higher than 0.8. Other unstructured meshes follow the same distribution. Spatial numerical schemes commit interpolation and approximation errors while transporting the velocity and the temperature variables. A poor grid quality will increase these errors, leading to more numerical diffusion errors and so affecting the results.

Moreover, while YALES2 spatial numerical scheme are $4th$ order, this is only true on uniform and regular grid. Due to the cell size variations of the $U3$ mesh, this integration drops to $3rd$ order, leading to higher numerical error level and so may cause different flow behaviour. Finally estimating the flux at the wall is known to be quite an arduous task. For unstructured grids, the estimation gets even more complex if the mesh is irregular, causing face-to-face flux irregularities related to the wall mesh. Because of these three sources of error, each grid type simulation deviates from each other, ending on different wall fluxes and as a result different velocity and temperature fields.

Nevertheless, it can concluded that both structured and unstructured grids simulations are correctly reproducing the SBL of the GABLS1 configuration. All studied quantities are well within previous studies data spread. Minor differences between $S3$ and $U3$ have been highlighted particularly in the wall heat flux and three sources of error have been highlighted: the grid quality, the order of the numerical schemes and the accuracy of the flux estimation.

3.2. Sensitivity to resolution

After assessing the impact of the use of unstructured meshes on a recommended mesh resolution, the impact of the grid resolution on the simulation results is now studied. Hence, a sensitivity to resolution study with a grid resolution varying from $\Delta x = 12.5\,\mathrm{m}$ to $\Delta x = 2\,\mathrm{m}$ is performed. Simulations are referred as $S1$ to $S4$ and $U1$ to $U4$ for structured and unstructured grids,

Preprint not peer reviewed

This preprint research paper has not been peer reviewed. Electronic copy available at: https://ssrn.com/abstract=4995353

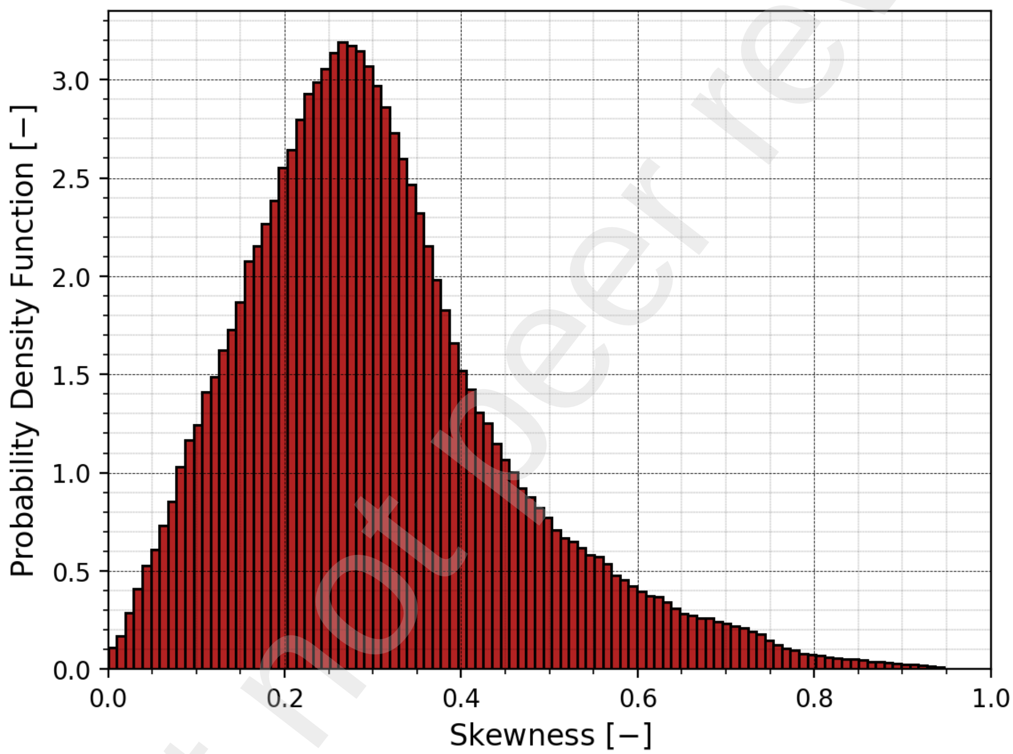

Figure 6: Probability density function (PDF) of the skewness distribution for $U3$ mesh.

Preprint not peer reviewed

This preprint research paper has not been peer reviewed. Electronic copy available at: https://ssrn.com/abstract=4995353

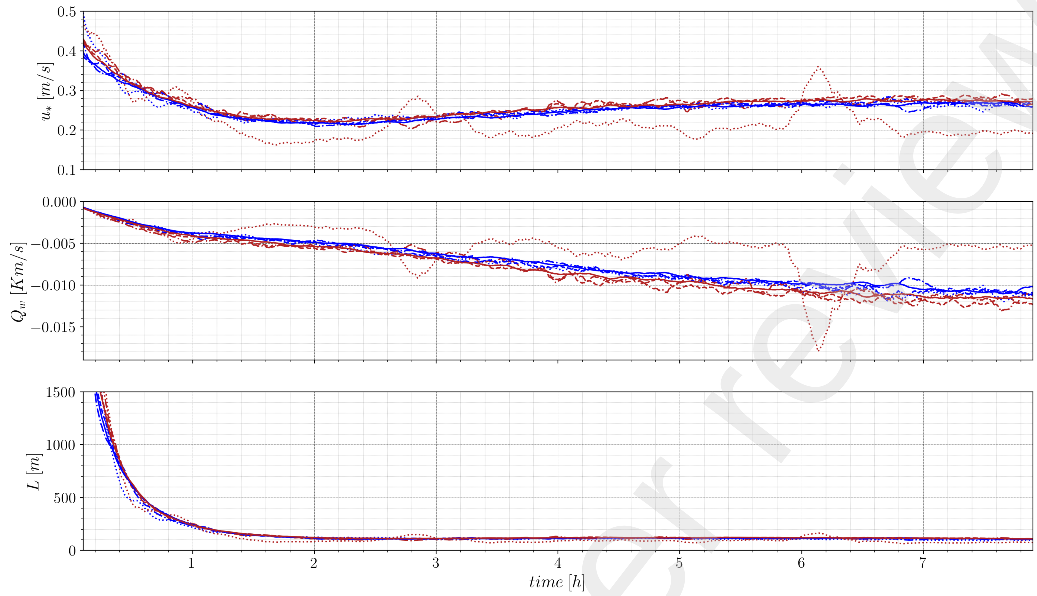

Figure 7: Frictional velocity, wall heat flux and Monin-Obukhov length time series. Blue and red lines stand for structured and unstructured grids, respectively. 4 resolutions are plotted: $\Delta x = 12.5\,\mathrm{m}$ (·····), $\Delta x = 6.25\,\mathrm{m}$ (-·-·), $\Delta x = 3.125\,\mathrm{m}$ (- - -) and $\Delta x = 2\,\mathrm{m}$ (——).

respectively. Each number corresponds to the resolution level according to Tab. 1.

Wall integrated quantities time series are shown in Fig. 7. All results behave similarly except for $U1$, which gives results that are irrelevant. While the friction velocities for the structured grid simulations show slightly lower and more noisy values, the differences in the wall heat flux are more pronounced. Unstructured grids simulations show a greater heat flux with respect to the structured grids. This difference has an impact on the temperature, velocity and flux profiles as seen in Section 3.1. However, finer meshes tend to converge to a similar value, although not perfectly matching, reducing the numerical diffusion and allowing for better gradient estimation. This behaviour supports the destabilization process influence caused by numerical error as the source of the gap between the two grid types. For the Monin-Obukhov length, which is a more global variable, all simulations are nearly identical.

Figs. 8 and 9 show instantaneous velocity and temperature planes, re-

Preprint not peer reviewed

This preprint research paper has not been peer reviewed. Electronic copy available at: https://ssrn.com/abstract=4995353

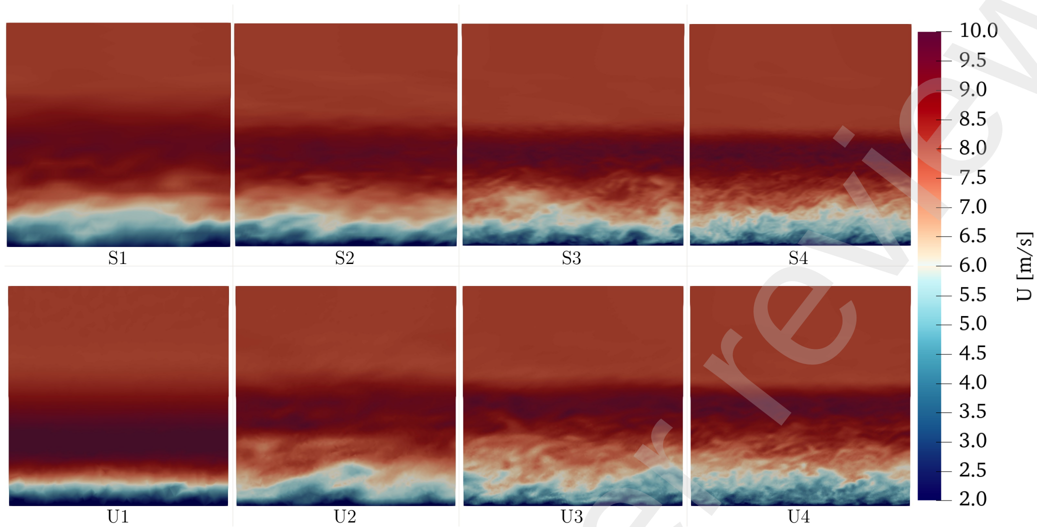

Figure 8: XZ velocity planes at $Y = 200\,\mathrm{m}$. Top: structured cases, bottom: unstructured cases. From left to right mesh resolution increases.

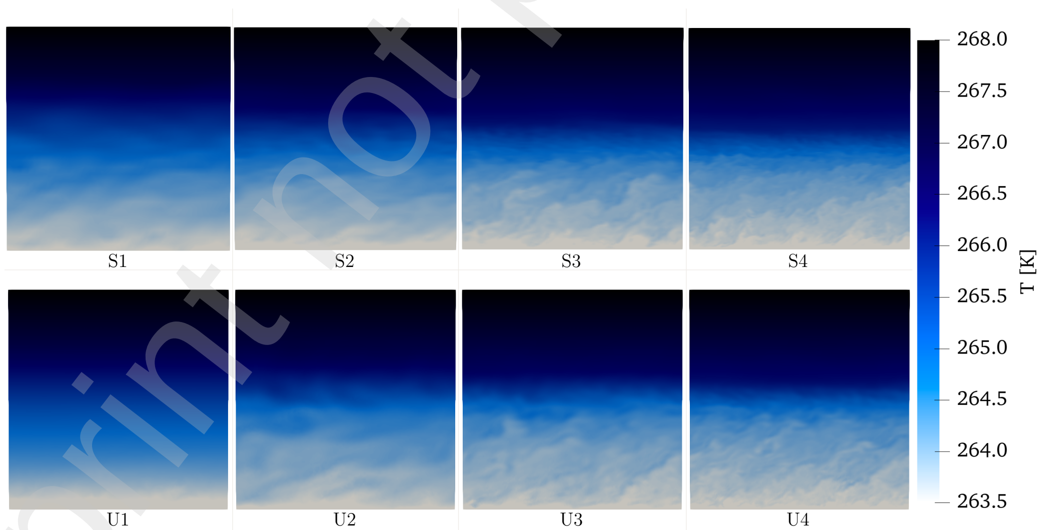

Figure 9: XZ temperature planes at $Y = 200\,\mathrm{m}$. Top: structured cases, bottom: unstructured cases. From left to right mesh resolution increases.

Preprint not peer reviewed

This preprint research paper has not been peer reviewed. Electronic copy available at: https://ssrn.com/abstract=4995353

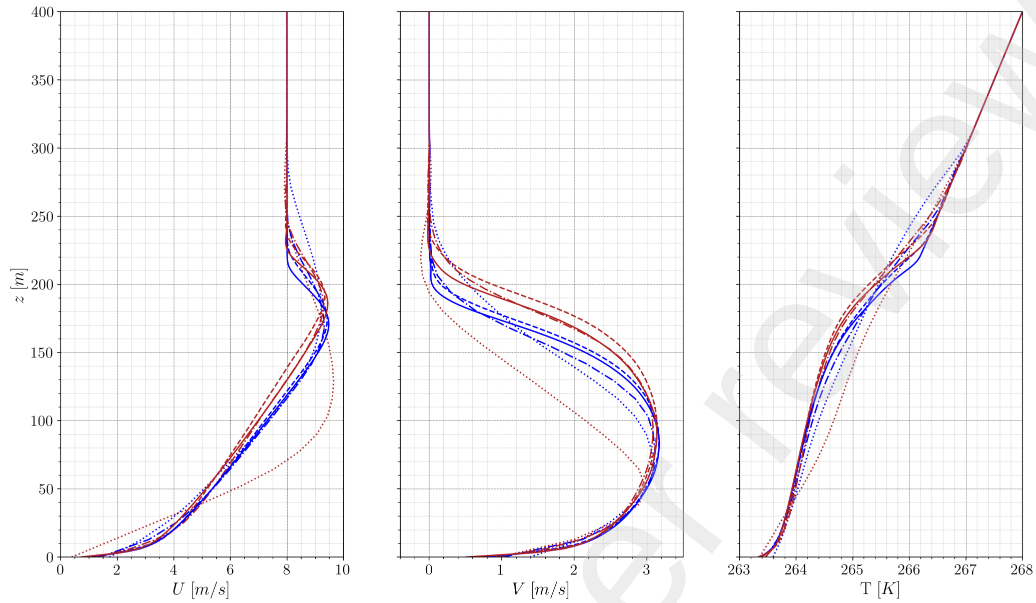

Figure 10: Average velocity and temperature profile. Blue and red lines stand for structured and unstructured grids, respectively. 4 resolutions are plotted: $\Delta x = 12.5\,\text{m}$ (·····), $\Delta x = 6.25\,\text{m}$ (-·-·), $\Delta x = 3.125\,\text{m}$ (- - -) and $\Delta x = 2\,\text{m}$ (——).

spectively. These planes are normal to the Y direction, at $Y = 200\,\text{m}$. This qualitative display shows the impact of the mesh resolution on the flow. By refining, more vortices are captured. At a glance, there is a noticeable difference between the resolution levels, but not between the structured and unstructured cases.

Figure 10 presents the velocity and temperature profiles spatially averaged over horizontal planes and temporally averaged between the $7th$ and $8th$ hour. Again, except for $U1$, all other grids show similar behaviour. The trend highlighted in Section 3.1, where the unstructured grid has a temperature inflection above the one of the structured case, is confirmed for all resolutions. The streamwise and tangential velocities return to the geostrophic wind at higher altitudes.

The momentum and heat flux profiles for all meshes are shown in Fig. 11. For all resolutions except the coarsest, the unstructured grids exhibit stronger fluxes. For the coarsest resolution, fluxes are near zero because the flow behaviour is far from expected with a boundary layer that no longer resembles a stable atmospheric layer. Fluxes are stronger with a finer mesh with both

Preprint not peer reviewed
This preprint research paper has not been peer reviewed. Electronic copy available at: https://ssrn.com/abstract=4995353

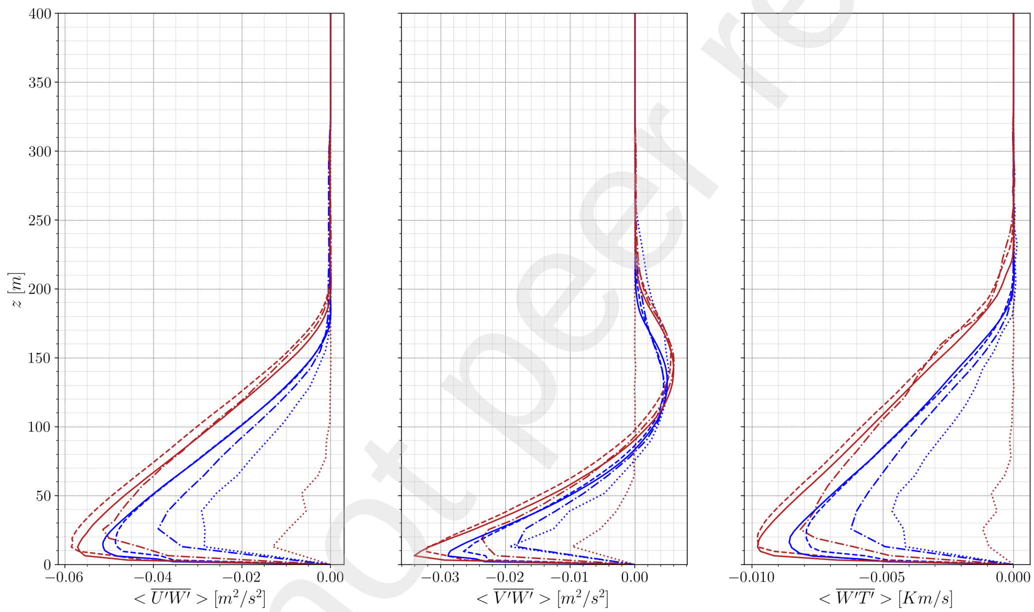

Figure 11: Average momentum and heat fluxes profile. Blue and red lines stand for structured and unstructured grids, respectively. 4 resolutions are plotted: $\Delta x = 12.5\,\mathrm{m}$ (·····), $\Delta x = 6.25\,\mathrm{m}$ (-·-·), $\Delta x = 3.125\,\mathrm{m}$ (- - -) and $\Delta x = 2\,\mathrm{m}$ (——).

Preprint not peer reviewed

This preprint research paper has not been peer reviewed. Electronic copy available at: https://ssrn.com/abstract=4995353

structured and unstructured grids. As expected, a finer grid is less dissipative and captures more turbulent kinetic energy. Again, the difference in wall heat fluxes leads to differences in momentum and heat fluxes profiles along the height. Stronger heat flux observed with the unstructured grid simulations leads to more fluctuations. Finally, all cases give satisfactory results except the structured and unstructured coarsest meshes, which will not be further considered into the analysis.

The boundary layer height was measured to evaluate the LES quality [12]. The calculation of the boundary layer height is based on the turbulent stress [11]. Its disappearance means a transition to a non-turbulent layer, i.e. the top of the ABL. It is worth noting that the calculation of the boundary layer height is often based on the heat flux. However, it may be inaccurate if the heat flux is affected by gravity waves, which predominate at the top of the ABL. Following this definition, the SBL top height is defined as the one where the tangential turbulent stress is reduced to $\alpha = 5\%$ of its surface value. Linear extrapolation is then used to evaluate the boundary layer height:

$$h = \frac{z|_{\langle \overline{U'W'} \rangle = \alpha u_*^2}}{1 - \alpha}. \tag{9}$$

Table 2 summarizes the boundary layer height from different studies with different codes and grid resolution. In both of our simulations as well as in other studies, the boundary layer heights tend to decrease with the grid resolution, converging towards $\sim 160 - 175$ m. As more turbulent fluctuations are captured as shown in Fig. 11. It is noted that simulations based on unstructured grids provide a boundary layer that is 10% higher.

The original GABLS1 study [12] used their most refined mesh simulations, with a grid cell size of $\Delta x = 1$ m, as references. The average boundary layer height at this resolution is 157 m. Compared to this reference, all computations showing an ABL height difference of less than 20% are considered accurate. Following this criterion, both structured and unstructured grids present an accurate behaviour, i.e. from 3.8% to 2.5% deviation for the structured grid and from 18% to 14% deviation for the unstructured one. This is in line with the original study advised requirements: a minimum grid length of $\Delta x = 6.25$ m to obtain a stable boundary layer height accuracy of 20%.

Quantifying the height of the boundary layer is essential, but not sufficient. While interesting, a similar boundary layer height does not reflect the

Preprint not peer reviewed
This preprint research paper has not been peer reviewed. Electronic copy available at: https://ssrn.com/abstract=4995353

Δx [m]	12.5	6.25	3.125	2
GABLS1 [12]	215	188	182	174
Cuxart et al. [37] - LES	-	-	177	-
Stoll and Porté-Agel [38]	-	-	173	-
Huang and Bou-Zeid [16]	-	-	-	158
Abkar and Moin [34]	168	165	169	-
Gadde et al. [19]	-	-	-	$166 - 176$
Min et al. [14]	-	-	160	-
Current work - Unstructured	149	180	186	179
Current work - Structured	149	163	162	161

Table 2: Boundary layer heights in various studies, depending on the grid resolution.

		Δx [m]			
Mesh type	Quantity	12.5	6.25	3.125	2
Unstructured	$\langle U \rangle$	9.2	4.8	5.9	4.6
	$\langle T \rangle$	0.09	0.08	0.09	0.07
Structured	$\langle U \rangle$	5.3	2.9	2.7	1.9
	$\langle T \rangle$	0.09	0.06	0.05	0.03

Table 3: Relative $L2$ norm error in % of the horizontal average velocity and temperature profiles compared to the reference profiles from [12].

Preprint not peer reviewed

This preprint research paper has not been peer reviewed. Electronic copy available at: https://ssrn.com/abstract=4995353

global behaviour of the boundary layer or the amplitude of the over-speed region. To be more quantitative in this respect, another criterion have been used. The relative $L2$ norm error. The simulation designed as a reference in [12] have been used as reference. The relative $L2$ norm error have been measured on horizontal average velocity and temperature profiles. Values are gathered in Tab 3. Excluding the coarsest meshes, the $L2$ norm error on streamwise velocity does not exceed 6%, while on temperature it remains under 0.1%. By refining the mesh, the $L2$ norm error decreases but is within an enveloppe, showing a grid convergence below $\Delta x = 6.25\,\mathrm{m}$. Overall, the obtained results present a very good agreement to the original study, proving the validity of the methodology to correctly reproduce the stable atmospheric boundary layer dynamics.

4. Conclusions and openings

A high-order incompressible Navier-Stokes solver able to perform LES of a stable boundary layer on unstructured meshes was developed, which is not straightforward. It takes into account the Coriolis force, the Boussinesq approximation for buoyancy-driven flows and the Monin-Obukhov similarity theory for wall modeling. This framework was validated against the GABLS1 setup. Time-averaged and variance of quantities like velocity, temperature and fluxes were compared with both structured and unstructured meshes of similar advised homogeneous cell size $\Delta x = 3.125\,\mathrm{m}$. Very good agreement was obtained with both meshes compared to the initial and to more recent studies. Minor differences between the two setups were highlighted: the unstructured grid produces slightly more numerical diffusion of the temperature scalar than the structured grid.

Moreover, the gradient estimation is also more difficult in the unstructured formalism, leading to a less accurate prediction of the flux. As a consequence, the destabilization of the stable boundary layer occurs differently, resulting in a slight gap between the results at the end of the simulation. The boundary layer height is 10% higher with the unstructured grid, with stronger velocity variances as momentum and heat fluxes. However, these differences remain small compared to the range of results from other studies. It appears that the subgrid scale models [19], numerical methods [10, 20], and grid resolutions [35] have more influence on the results than the use of an unstructured grid.

Preprint not peer reviewed

This preprint research paper has not been peer reviewed. Electronic copy available at: https://ssrn.com/abstract=4995353

A sensitivity to grid resolution study was also performed. The boundary layer height was measured and showed that a grid length of $\Delta x = 6.25\,\mathrm{m}$ is sufficient to obtain a 20% accuracy. The relative $L2$ norm errors of streamwise velocity and temperature profiles to a reference high resolution study were also calculated for both structured and unstructured grids with less than 6% for both meshes. Thus, a $\Delta x = 6.25\,\mathrm{m}$ grid size for both structured and unstructured meshes is sufficient to produce a simulation with a reasonable accuracy, but a $\Delta x = 3.125\,\mathrm{m}$ grid size is ideal for a robust LES.

To conclude, properly reproducing a stable boundary layer using unstructured grid has been performed for the first time to the author's knowledge. More geometrically complex cases will then be investigated where structured grids are unqualified like complex terrain simulations.

acknowledgements

This work has been initiated during the Extreme CFD Workshop & Hackathon (https://ecfd.coria-cfd.fr). This project was provided with computer and storage resources by GENCI at TGCC thanks to the grant 2023-A0142A11335 on the supercomputer Joliot Curie's ROME partition and to CRIANN resources under the allocation 2012006.

Appendix 1: GABLS1 source of errors

Two sources of debate can be highlighted in the design of the GABLS1 benchmark [12]: initial condition definition and numerical errors accumulation.

Initial condition definition
. The initial condition vertical temperature profile of the GABLS1 benchmark is spatially uniform, set to $T = 265\,\mathrm{K}$ from the ground up to $z = 100\,\mathrm{m}$ and then increases by $1\,\mathrm{K}/100\,\mathrm{m}$. To help the flow destabilization process, a random potential temperature perturbation of $0.1\,\mathrm{K}$ amplitude is superposed to the profile between $z = 0\,\mathrm{m}$ and $z = 50\,\mathrm{m}$. The definition of this random perturbation is left to the user's discretion, which is questionable. Commonly, users add a randomly generated noise on each control volume which is spatially uncorrelated. This can clearly have an impact on the flow evolution and will depends on the mesh resolution and grid partitioning.

Preprint not peer reviewed

This preprint research paper has not been peer reviewed. Electronic copy available at: https://ssrn.com/abstract=4995353

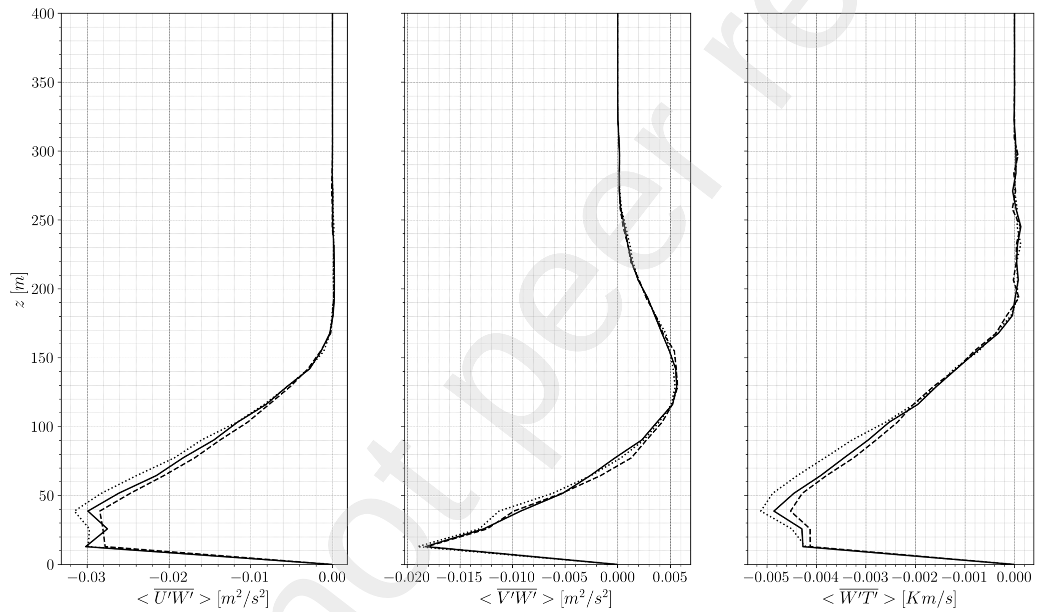

Figure 12: Horizontally averaged momentum and heat fluxes vertical profile s on S3 mesh. Results with seed 1 and 1 CPU core (—), seed 2 and 1 CPU Core (- - -) and seed 1 and 4 CPU cores(·····).

Preprint not peer reviewed

This preprint research paper has not been peer reviewed. Electronic copy available at: https://ssrn.com/abstract=4995353

To quantify its impact on the flow behaviour, two identical simulations based on the $\Delta x = 12.5\,\mathrm{m}$ structured grid are performed with the only difference being the random number seeds. Figure 12 shows the momentum and heat fluxes profiles spatially averaged over horizontal planes and temporally averaged between the $7th$ and the $8th$ hour, so long after initialization. Results present a clear dependency on the random seed, with noticeable differences, showing a different flow evolution between the initialisation and the $8th$ hour. Similar gaps are observed for average velocity, temperature and velocity variance and these results are reproducible for different grid resolutions and numerical schemes, but not shown here for the sake of clarity.

This effect means that a small change in the initial profile affect the behaviour of the flow ans so the collected statistics. It can distort the comparison between codes since the random number generation will necessarily be different. Moreover, this random number is only determined by an amplitude and a mean, analogous to a white noise without spatial coherence. As different grid resolution were used in all GABLS1 studies, different fluctuation frequency were added. Since the flow behaviour is sensitive to this initial profile, part of the differences obtained when comparing two resolutions can be explained by this phenomenon. Similarly, it could also explain differences between structured and unstructured grids. Adding constraints on the random number, such as giving the fluctuation frequency or giving some spatial correlation, would help in having similar initial condition, whatever the mesh type and resolution. The perturbation would then be analogous to pink noise instead of white noise. The results would still depend on the random number seed but at least would minimize differences when comparing different resolutions.

Numerical errors accumulation

. Theoretically, a deterministic behaviour of the simulation is expected, since the resolution of the Navier-Stokes equations is fully deterministic. Simulations are reproducible and all states can be derived from the input data. However, numerical errors can lead to non-deterministic flows, i.e. different results can be obtained with identical input data. The sources of numerical errors are various: node reordering, machine precision, operation orders, etc. In this respect, the grid partitioning and so the number of CPU cores used in a LES can cause variations in the results. It has been demonstrated that the propagation of numerical errors is linear for laminar flows but exponential for turbulent flows [39]. This difference between laminar and turbulent flows

Preprint not peer reviewed

This preprint research paper has not been peer reviewed. Electronic copy available at: https://ssrn.com/abstract=4995353

is due to the true chaotic nature of turbulence.

To illustrate this effect, two identical simulations were performed on the $\Delta x = 12.5\,\mathrm{m}$ structured grid with different number of CPU cores: one simulation with 1 CPU, the other with 4 CPUs and by keening the same random generator seed). Figure 12 shows the momentum and heat fluxes profiles for both cases. Momentum and heat fluxes profiles show discrepancies depending on the number of CPUs used. Similar gaps are observed for other quantities and is reproducible with other grid resolutions and numerical schemes but are not shown fot the sake of brevety. As the errors accumulate quickly, working with higher machine precision will not suppress the error propagation but only delay it. Since error propagation is exponential, the flow paths will always diverge [39]. To circumvent this effect, several simulations with different random number generations could be performed and averaged to give more statistical accuracy.

References

[1] IRENA 2019 *Future of wind: Deployment, investment, technology, grid integration and socio-economic aspects*

[2] Veers P, Dykes K, Lantz E, Barth S, Bottasso C L, Carlson O, Clifton A, Green J, Green P, Holttinen H *et al.* 2019 *Science* **366** eaau2027

[3] Kaimal J C and Finnigan J J 1994 *Atmospheric boundary layer flows: their structure and measurement* (Oxford university press)

[4] Porté-Agel F, Bastankhah M and Shamsoddin S 2020 *Boundary-Layer Meteorology* **174** 1–59

[5] Doubrawa P, Debnath M, Moriarty P J, Branlard E, Herges T G, Maniaci D and Naughton B 2019 Benchmarks for model validation based on lidar wake measurements *Journal of Physics: Conference Series* vol 1256 (IOP Publishing) p 012024

[6] Moriarty P, Hamilton N, Debnath M, Herges T, Isom B, Lundquist J K, Maniaci D, Naughton B, Pauly R, Roadman J *et al.* 2020 American wake experiment (awaken) Tech. rep. Lawrence Livermore National Lab.(LLNL), Livermore, CA (United States ...

Preprint not peer reviewed

This preprint research paper has not been peer reviewed. Electronic copy available at: https://ssrn.com/abstract=4995353

[7] Stoll R, Gibbs J A, Salesky S T, Anderson W and Calaf M 2020 *Boundary-Layer Meteorology* **177** 541–581

[8] Garratt J R 1994 *Earth-Science Reviews* **37** 89–134

[9] Holtslag A, Svensson G, Basu S, Beare B, Bosveld F and Cuxart J 2012 Overview of the gewex atmospheric boundary layer study (gabls) *Proceedings of the Workshop on Diurnal cycles and the stable boundary layer, 7-10 November 2011, Reading, UK* pp 11–23

[10] Sanz Rodrigo J, Churchfield M and Kosovic B 2017 *Wind Energy Science* **2** 35–54

[11] Kosović B and Curry J A 2000 *Journal of the atmospheric sciences* **57** 1052–1068

[12] Beare R J, Macvean M K, Holtslag A A, Cuxart J, Esau I, Golaz J C, Jimenez M A, Khairoutdinov M, Kosovic B, Lewellen D *et al.* 2006 *Boundary-Layer Meteorology* **118** 247–272

[13] Sullivan P P, Weil J C, Patton E G, Jonker H J and Mironov D V 2016 *Journal of the Atmospheric Sciences* **73** 1815–1840

[14] Min M and Tombouldies A 2022 Simulating atmospheric boundary layer turbulence with nek5000/rs Tech. rep. Argonne National Laboratory (ANL), Argonne, IL (United States)

[15] Kumar V, Svensson G, Holtslag A, Meneveau C and Parlange M B 2010 *Journal of Applied Meteorology and Climatology* **49** 1496–1516

[16] Huang J and Bou-Zeid E 2013 *Journal of the Atmospheric Sciences* **70** 1513–1527

[17] Matheou G and Chung D 2014 *Journal of the Atmospheric Sciences* **71** 4439–4460

[18] Ghaisas N S, Archer C L, Xie S, Wu S and Maguire E 2017 *Wind Energy* **20** 1227–1240

[19] Gadde S N, Stieren A and Stevens R J 2021 *Boundary-Layer Meteorology* **178** 363–382

Preprint not peer reviewed

This preprint research paper has not been peer reviewed. Electronic copy available at: https://ssrn.com/abstract=4995353

[20] Lazeroms W 2015 *Turbulence modelling applied to the atmospheric boundary layer* Ph.D. thesis KTH Royal Institute of Technology

[21] Moureau V, Domingo P and Vervisch L 2011 *Comptes Rendus Mécanique* **339** 141–148

[22] Kraushaar M 2011 *Application of the compressible and low-Mach number approaches to Large-Eddy Simulation of turbulent flows in aero-engines* Theses Institut National Polytechnique de Toulouse - INPT URL `https://tel.archives-ouvertes.fr/tel-00711480`

[23] Gray D D and Giorgini A 1976 *International Journal of Heat and Mass Transfer* **19** 545–551

[24] Monin A S and Obukhov A M 1954 *Contrib. Geophys. Inst. Acad. Sci. USSR* **151** e187

[25] Landau L and Lifshitz E 1959 *Section 92, problem* **2**

[26] Businger J 1971 *Journal of the atmospheric Sciences* **28** 181–189

[27] Högström U 1988 Non-dimensional wind and temperature profiles in the atmospheric surface layer: A re-evaluation *Topics in Micrometeorology. A Festschrift for Arch Dyer* (Springer) pp 55–78

[28] Basu S, Holtslag A A, Van De Wiel B J, Moene A F and Steeneveld G J 2008 *Acta Geophysica* **56** 88–99

[29] Ypma T J 1995 *SIAM review* **37** 531–551

[30] Larsson J, Kawai S, Bodart J and Bermejo-Moreno I 2016 *Mechanical Engineering Reviews* **3** 15–00418

[31] Germano M, Piomelli U, Moin P and Cabot W H 1991 *Physics of Fluids A: Fluid Dynamics* **3** 1760–1765

[32] Lilly D K 1992 *Physics of Fluids A: Fluid Dynamics* **4** 633–635

[33] Pope S B 2001 *Measurement Science and Technology* **12** 2020–2021

[34] Abkar M and Moin P 2017 *Boundary-layer meteorology* **165** 405–419

Preprint not peer reviewed

This preprint research paper has not been peer reviewed. Electronic copy available at: https://ssrn.com/abstract=4995353

[35] Dai Y, Basu S, Maronga B and de Roode S R 2021 *Boundary-Layer Meteorology* **178** 63–89

[36] Audusse E, Do M H, Omnes P and Penel Y 2018 *Journal of Computational Physics* **373** 91–129

[37] Cuxart J, Holtslag A A, Beare R J, Bazile E, Beljaars A, Cheng A, Conangla L, Ek M, Freedman F, Hamdi R *et al.* 2006 *Boundary-Layer Meteorology* **118** 273–303

[38] Stoll R and Porté-Agel F 2008 *Boundary-layer meteorology* **126** 1–28

[39] Garciá M 2008 *Méthodes numériques pour la simulation aux grandes échelles de la combustion gazeuse et diphasique* Ph.D. thesis institut national polytechnique de Toulouse

Preprint not peer reviewed

This preprint research paper has not been peer reviewed. Electronic copy available at: https://ssrn.com/abstract=4995353